Postsynaptic receptors regulate presynaptic neurotransmitter stability

Swetha K. Godavarthi[1,2], Masaki Hiramoto[3], Yuri Ignatyev[4], Jacqueline B. Levin[5], Huiquan Li[1,2], Marta Pratelli[1,2], Jennifer Borchardt[6], Cynthia Czajkowski[6], Laura N. Borodinsky[5], Lora Sweeney[4], Hollis T. Cline[3], Nicholas C. Spitzer[1,2]

[1]Neurobiology Department, University of California San Diego, USA

[2]Kavli Institute for Brain & Mind, University of California San Diego, USA

[3]Neuroscience Department, The Scripps Research Institute, La Jolla CA, USA

[4]Institute of Science and Technology Austria, Austria

[5]Department of Physiology & Membrane Biology, Shriners Hospital for Children, Northern California; University of California Davis, School of Medicine, USA

[6]Neuroscience Department, University of Wisconsin Madison, USA

Abstract

Alteration of the electrical activity of the nervous system causes plasticity in neural circuits. Many of the changes occur at synapses[1–3]. For example, neurotransmitter switching involves changes in the identity of presynaptic neurotransmitters and corresponding changes in postsynaptic transmitter receptors, thereby achieving a match between the transmitter and its cognate receptor. However, it is unknown whether changes in postsynaptic receptors can regulate presynaptic transmitters. Here we address this question at the developing neuromuscular junction. We find that blockade of endogenous postsynaptic acetylcholine receptors leads to loss of the cholinergic phenotype in motor neurons and the reappearance and stabilization of an earlier, developmentally transient glutamatergic phenotype. In addition, exogenous postsynaptic expression of $GABA_A$ receptors leads to the appearance and stabilization of an earlier, transient GABAergic motor neuron phenotype. Thus, acetylcholine receptors are necessary to stabilize acetylcholine as a transmitter, and $GABA_A$ receptors are sufficient to stabilize GABA as a transmitter. GARLH4 links the $GABA_A$ receptor to neuroligin, and Lrp4 links the acetylcholine receptor to dystroglycan through rapsyn and MUSK. Both neuroligin and dystroglycan bind to neurexin, which in turn binds to forms of the CASK transcription factor in motor neurons. Knock

down of GARLH4 or Lrp4 postsynaptically or CASK presynaptically blocks stabilization of the GABAergic and cholinergic phenotypes. These results implicate transsynaptic bridges in establishing receptor-dependent stability of the cognate neurotransmitters. Our findings provide opportunities to investigate a role for dysfunctional transmitter receptors in neurological disorders that involve the loss of the presynaptic transmitter.

Main

Postsynaptic receptors at neuronal synapses are often viewed as passive responders to presynaptic neurotransmitters. In the case of transmitter switching, the presynaptic neuron has appeared to be the primary responder, with the postsynaptic cell responding by expressing the matching receptor[4–7]. Is it also possible for changes in the receptors on postsynaptic cells to alter transmitter expression in their presynaptic neurons? Robust communication requires both the sender's message to the receiver and the receiver's acknowledgment to the sender that the message has been received. The acknowledgment signal assures the fidelity of information transfer. Activity-driven retrograde signaling by endocannabinoids and neurotrophins from the postsynapse regulates presynaptic neuron survival, dendrite formation and growth, and synaptogenesis[8,9]. It is unclear whether transmitter receptors regulate properties of their presynaptic transmitter. Here we demonstrate that retrograde signaling by postsynaptic neurotransmitter receptors is necessary and sufficient to stabilize expression of their cognate neurotransmitter in the presynaptic neuron.

Blocking endogenous acetylcholine receptors

We first tested whether blockade of acetylcholine receptors (AChR) of cholinergic neuromuscular junctions in *Xenopus* embryos affects the expression of acetylcholine in motor neurons. Agarose beads containing AChR antagonists, pancuronium or curare, were implanted into developing mesoderm at 1 day post fertilization (dpf) (stages 18-21) for local diffusive drug delivery (**Fig. 1a**). Embryos were wholemount immunostained for choline acetyltransferase (ChAT), the enzyme that synthesizes ACh, and for synaptic vesicle protein 2 (SV2), a marker of nerve terminals, at 2, 3, 4 and 7 dpf (stages 36, 41, 43 and 47) to determine the capacity of nerve terminals for ACh

synthesis. At 2 dpf, the labeled area of ChAT+SV2+ motor neuron terminals running along the myocommatal junctions at the boundaries between chevrons of myocytes within 100 µm of pancuronium-loaded beads was not different from the labeled area in saline controls (**Fig. 1b,c**). By 3 dpf, ChAT+ area had decreased to 19% of controls with no change in the SV2+ area. By 4 dpf the area had fallen to 5% of saline controls (**Fig. 1d,f,h**), with significant decline in corresponding SV2+ staining (**Fig. 1e,g,i; Suppl Fig. 1; Suppl Fig. 2; Suppl Fig. 3**). These results suggest that the loss of ChAT precedes the loss of nerve terminals and that some function of postsynaptic AChR is required for the stability of ChAT expression. Interestingly, the loss of AChR precedes the loss of nerve terminals in a mouse model of myasthenia gravis (MG)[10]. MG is often the result of an autoimmune attack on AChR function[11–13]. Our findings suggest that reduced levels of presynaptic ACh, in addition to loss of AChR, could contribute to the ensuing muscle fatigue, also observed in congenital MG resulting from ChAT deficiency[12].

Normally, embryonic motor neurons express glutamate in their cell bodies at 1 dpf and its level decreases by 2 dpf as ChAT begins to be detected[14]. By 3 dpf glutamate is no longer detected immunohistochemically. Blockade of AChR with pancuronium led to increased expression of a vesicular glutamate transporter (VGLUT1) in motor neuron terminals within 100 µm of a bead (**Fig. 1j; Suppl Fig. 4**), indicating the reappearance and stabilization of a glutamatergic phenotype. The reappearance of VGLUT1 was accompanied by a corresponding increase in expression of glutamatergic AMPA and NMDA receptor subunits in myocytes (**Fig. 1k,l**). Intracellular recordings from these myocytes at 4 dpf yielded two classes of mEPPs, recognized by their rise and decay times (**Fig. 1m-v**). Rapid rise-rapid decay mEPPs were blocked by NBQX, indicating that they depended on AMPA receptors. Only the smaller mEPPs remained after the NBQX block, with slower rise and decay times typical of AChR. These mEPPs were eliminated by the additional application of pancuronium. The local block of AChR did not result in immunostaining for GABA (**Suppl Fig. 5**)**.** This result is consistent with the earlier report of increase in the number of neurons expressing glutamate and ionotropic glutamate receptors, but not GABA or glycine, that occurs following a reduction in neuronal activity[4,15].

Expressing exogenous GABA receptors

During development, embryonic motor neurons express GABA as well as glutamate in their cell bodies and in their axons[14]. Ordinarily, the level of GABA decreases by 2 dpf as ChAT appears, and GABA has disappeared by 3 dpf (**Suppl Fig. 6**). We expressed $GABA_A$ receptors in a small number of embryonic myocytes[16] to ask whether this would stabilize expression of GABA in the motor neurons that innervate these myocytes. To generate $GABA_AR$ in myocyte membranes, we injected the V2.1 blastomere at the 4-cell stage with α1-EGFP, β2, and γ2 $GABA_A$ receptor subunit transcripts. α1-EGFP-only transcripts served as control, as expression in this case is restricted to the cytoplasm and does not appear in the plasma membrane[17] (**Suppl Fig. 7**). The GFP-tag on the α1 subunit permitted the transfected myocytes to be identified. Strikingly, at 3 dpf, expression of $GABA_AR\alpha\beta\gamma$ receptors in myocytes, but not $GABA_AR\alpha$ alone, led to expression of SV2, GABA and VGAT in the nerve terminals that innervate them (**Fig. 2; Suppl Fig. 8**). ChAT was coexpressed with GABA and VGAT, suggesting that the terminals are in fact processes of motor neurons (**Suppl Fig. 9a-h**). Further support that the nerve terminals expressing GABA and VGAT are from motor neurons came from the observation that GABA and motor neuron transcription factor Hb9, as well as GAD67 and ChAT, are coexpressed in neuronal cell bodies (**Suppl Fig. 9i-l**). Moreover, motor neurons expressing ChAT and GABA expressed the motor neuron transcription factor lim3, demonstrating that the motor neurons are from the medial motor column pool formed by the primary wave of neurogenesis and not from rAdlh1a2-expressing neurons of the lateral motor column pool, which appear later (**Suppl Fig. 10**). Expression of $GABA_AR\alpha\beta\gamma$ stabilized the GABAergic phenotype but did not stabilize expression of VGLUT1 or glycine in innervating axons (**Suppl Fig. 11**).

The expression of GABA in motor neuron axons at 2 dpf in these embryos was increased specifically in axons contacting myocytes expressing $GABA_AR\alpha\beta\gamma$. Myocytes expressing $GABA_AR\alpha$ did not show this increase (**Suppl Fig. 12**), indicating that GABA was stabilized by the presence of the cognate postsynaptic receptor. The increase and stabilization of GABA in axons innervating $GABA_AR\alpha\beta\gamma$-expressing myocytes continued until at least 7 dpf (**Suppl Fig. 13**). To further test whether $GABA_AR\alpha\beta\gamma$-expressing myocytes were specific in stabilizing the presynaptic GABAergic

phenotype, we removed the mesoderm of 15 hours post fertilization (hpf) (stage 13-14) wild type embryos and transplanted, into these hosts, 15 hpf mesoderm grafts expressing $GABA_AR\alpha\beta\gamma$ or $GABA_AR\alpha$. Only axons that contacted $GABA_AR\alpha\beta\gamma$-expressing myocytes in the grafts expressed GABA and SV2 (**Suppl Fig. 14**). Thus, stabilization of GABA depended on these myocytes and not on GABA expression within the spinal cord.

To assess the functional consequence of anatomical innervation by nerve terminals expressing both ChAT and GABA, we recorded miniature endplate potentials (mEPPs) from $GABA_AR\alpha\beta\gamma$-expressing myocytes at 4 dpf. We observed two classes of mEPPs, distinguished on the basis of their rise and decay times and their frequency[4]. Those with faster times occurred at a mean frequency of 0.6±0.0 sec^{-1} and were blocked by pancuronium, showing they depended on AChR. Those with slower times occurred at a mean frequency of 0.2±0.0 sec^{-1} and were blocked by bicuculline (**Fig. 3a-c**), indicating they depended on GABA. Mean rise and decay times in the presence of pancuronium were 6.0 and 11.0 ms, but were 3.9 and 5.0 ms in the presence of bicuculline (**Fig. 3d-f**). In contrast, only a single class of mEPPs at a frequency of 1.0±0.1 sec^{-1} was observed when recording from myocytes that expressed $GABA_AR\alpha$. This value was significantly different from the frequency of cholinergic mEPPs recorded from the $GABA_AR\alpha\beta\gamma$-expressing myocytes that were blocked by pancuronium. These mEPPs had a mean rise time of 3.6 ms and a decay time of 4.5 ms (**Fig. 3g-j**), not different from the values of mEPPs recorded from $GABA_AR\alpha\beta\gamma$-expressing myocytes in the presence of bicuculline. The results of these recordings demonstrate that GABA can be functionally released from motor nerve terminals and innervate myocytes that express $GABA_AR\alpha\beta\gamma$ receptors.

Signal transduction by transsynaptic bridges

To understand the mechanism of retrograde signaling by which postsynaptic receptors regulate the stability of presynaptic transmitters, we considered the possible role of transsynaptic bridges. Presynaptic neurexins and postsynaptic neuroligins and dystroglycans are synaptic adhesion molecules (SAMs) that are important for proper maturation and function of synaptic contacts[18]. They bridge the synaptic cleft and create a potential pathway for retrograde signaling. However,

in tests of their properties, SAMs induced excitatory and inhibitory presynaptic specializations at the same time[19] and did not exhibit the specificity needed if transsynaptic bridges were to be relevant to our findings. Missing from these assays were the transmitter receptor itself and its co-receptors. The $GABA_AR\alpha\beta\gamma$ co-receptor protein GARLH4 mediates interaction between the γ subunit of the $GABA_AR\alpha\beta$ receptor and neuroligin 2, which binds to neurexin[20]. Postysynaptic expression of $GABA_AR\alpha\beta$ results in receptors with functional properties similar to those of $GABA_AR\alpha\beta\gamma$[17], but fails to stabilize presynaptic GABA; 0/12 $GABA_AR\alpha\beta$-expressing larvae express GABA in motor neuron axons contacting GFP-labeled myocytes and GABA expression remains restricted to the spinal cord. This finding indicates that the $GABA_AR$ γ subunit of the $GABA_AR\alpha\beta\gamma$ receptor, might act through a synaptic bridge to achieve presynaptic stability of the GABAergic phenotype.

To investigate directly how transsynaptic bridges might stabilize presynaptic transmitters, we first confirmed the presence of neurexin, neuroligin (**Suppl Fig. 15**) and dystroglycan[21] at the *Xenopus* neuromuscular junction. Knocking down GARLH4 in myocytes by injecting morpholinos into the V2.1 blastomere (**Suppl Fig. 16; Suppl Fig. 17**) prevented the $GABA_AR\alpha\beta\gamma$-mediated stabilization of GABA in motor neurons (**Fig. 4a-d**). This result suggested that the $GABA_AR$ γ subunit, in the $GABA_AR\alpha\beta\gamma$ receptor, mediates the expression of presynaptic GABA through GARLH4-neuroligin-neurexin transsynaptic bridges. Similarly, disrupting an AChR-rapsyn-Lrp4-musk-dystroglycan-neurexin transsynaptic bridge[22,23] by injecting morpholinos into the V2.1 blastomere to knock down the postsynaptic AChR co-receptor protein, Lrp4[24,25] (**Suppl Fig. 18**), recapitulated the destabilization and loss of ChAT that we observed in the presence of pancuronium (**Fig. 4e-l**). This result was corroborated by a significant reduction in the amplitude of cholinergic mEPPs in Lrp4 knock-down larvae in the presence of NBQX compared to control morpholino larvae (1.7±0.1 mV vs 2.7±0.1 mV; n^{mEPP}=177, N^{larvae}=7; $p<0.0001$, two-tailed t-test) and the detection of pancuronium-resistant NBQX-sensitive glutamatergic mEPPs in 4 dpf Lrp4 knock-down larvae (**Suppl Fig. 19**). Indeed, pancuronium may phenocopy the effect of knocking down Lrp4 by binding to the α and γ subunits of the AChR[26] and altering the AChR-Lrp4 interaction, thereby disrupting signaling through the cholinergic transsynaptic bridge.

We next considered CASK (Ca^{2+}/calmodulin-activated Ser-Thr kinase) as a candidate that could receive signals from the presynaptic ends of the transsynaptic bridges and stabilize transmitter expression in the motor neurons. CASK is a presynaptic membrane-associated guanylate kinase[27] (MAGUK) and transcription factor that binds to neurexin and is present at both glutamatergic[28] and GABAergic synapses[29]. We found that CASK is also expressed in the myotome of both wild type and $GABA_ARA\alpha\beta\gamma$-expressing *Xenopus* larvae (**Suppl Fig. 20**). CASK pre-mRNA is subject to alternative splicing that yields proteins with preferences to interact with many targets[30]. Autophosphorylated CASK translocates to the nucleus and induces transcription of genes essential for development[31,32]. Additionally, neurexin-1 competes as a CASK phosphorylation substrate, preventing CASK autophosphorylation[33]. The splice variants, together with differential phosphorylation, identified CASK as a potentially significant player in stabilizing presynaptic neurotransmitter expression. Knocking down presynaptic CASK by injecting morpholinos into the D1.2 blastomere to target the spinal cord (**Suppl Fig. 20**) disrupted both AChR-mediated ChAT stabilization and $GABA_AR\alpha\beta\gamma$-mediated GABA stabilization in motor neurons (**Fig. 4m-w**).

Discussion

Our results demonstrate that postsynaptic neurotransmitter receptors can regulate the stability of presynaptic neurotransmitters at newly formed neuromuscular junctions. Regulation is achieved by retrograde signaling that operates, we suggest, through transsynaptic bridges as acknowledgment (Ack) signals to the presynaptic motor neurons (**Fig. 4x**). Cholinergic synapses disappear when this Ack signal is blocked. GABAergic synapses are stabilized when the Ack signal is introduced. Neurexin serves as the final link of the transsynaptic bridge, receiving signals from the postsynaptic cell and transmitting them to achieve presynaptic cholinergic or GABAergic stabilization. It will be of interest to learn whether deficits in postsynaptic receptors and transsynaptic bridges contribute to reduced transmitter levels at neuronal synapses in the mature nervous system and to pathological change in neurological disorders.

References

1. Citri, A. & Malenka, R. C. Synaptic Plasticity: Multiple forms, functions, and mechanisms. *Neuropsychopharmacology* **33**, 18–41 (2008).
2. Turrigiano, G. G. & Nelson, S. B. Homeostatic plasticity in the developing nervous system. *Nat. Rev. Neurosci.* **5**, 97–107 (2004).
3. Spitzer, N. C. Neurotransmitter switching in the developing and adult brain. *Annu. Rev. Neurosci.* **40**, 1–19 (2017).
4. Borodinsky, L. N. & Spitzer, N. C. Activity-dependent neurotransmitter-receptor matching at the neuromuscular junction. *Proc. Natl. Acad. Sci.* **104**, 335–340 (2007).
5. Dulcis, D. & Spitzer, N. C. Illumination controls differentiation of dopamine neurons regulating behaviour. *Nature* **456**, 195–201 (2008).
6. Dulcis, D., Jamshidi, P., Leutgeb, S. & Spitzer, N. C. Neurotransmitter switching in the adult brain regulates behavior. *Science* **340**, 449–453 (2013).
7. Hammond-Weinberger, D. R., Wang, Y., Glavis-Bloom, A. & Spitzer, N. C. Mechanism for neurotransmitter-receptor matching. *Proc. Natl. Acad. Sci.* **117**, 4368–4374 (2020).
8. Castillo, P. E., Younts, T. J., Chávez, A. E. & Hashimotodani, Y. Endocannabinoid signaling and synaptic function. *Neuron* **76**, 70–81 (2012).
9. Harrington, A. W. & Ginty, D. D. Long-distance retrograde neurotrophic factor signalling in neurons. *Nat. Rev. Neurosci.* **14**, 177–187 (2013).

10. Rich, M. M., Colman, H. & Lichtman, J. W. In vivo imaging shows loss of synaptic sites from neuromuscular junctions in a model of myasthenia gravis. *Neurology* **44**, 2138–2138 (1994).

11. Peragallo, J. H. Pediatric myasthenia gravis. *Semin. Pediatr. Neurol.* **24**, 116–121 (2017).

12. Engel, A. G., Shen, X.-M., Selcen, D. & Sine, S. M. Congenital myasthenic syndromes: pathogenesis, diagnosis, and treatment. *Lancet Neurol.* **14**, 420–434 (2015).

13. Gilhus, N. E. & Verschuuren, J. J. Myasthenia gravis: subgroup classification and therapeutic strategies. *Lancet Neurol.* **14**, 1023–1036 (2015).

14. Root, C. M., Velazquez-Ulloa, N. A., Monsalve, G. C., Minakova, E. & Spitzer, N. C. Embryonically expressed gaba and glutamate drive electrical activity regulating neurotransmitter specification. *J. Neurosci.* **28**, 4777–4784 (2008).

15. Borodinsky, L. N. *et al.* Activity-dependent homeostatic specification of transmitter expression in embryonic neurons. *Nature* **429**, 523–530 (2004).

16. Moody, S. A. Fates of the blastomeres of the 16-cell stage Xenopus embryo. *Dev. Biol.* **119**, 560–578 (1987).

17. Connor, J. X., Boileau, A. J. & Czajkowski, C. A GABAA receptor alpha1 subunit tagged with green fluorescent protein requires a beta subunit for functional surface expression. *J. Biol. Chem.* **273**, 28906–11 (1998).

18. Südhof, T. C. Synaptic neurexin complexes: a molecular code for the logic of neural circuits. *Cell* **171**, 745–769 (2017).

19. Jiang, X., Sando, R. & Südhof, T. C. Multiple signaling pathways are essential for synapse formation induced by synaptic adhesion molecules. *Proc. Natl. Acad. Sci.* **118**, e2000173118 (2021).

20. Yamasaki, T., Hoyos-Ramirez, E., Martenson, J. S., Morimoto-Tomita, M. & Tomita, S. Garlh family proteins stabilize gabaa receptors at synapses. *Neuron* **93**, 1138-1152.e6 (2017).

21. Cohen, M., Jacobson, C., Godfrey, E., Campbell, K. & Carbonetto, S. Distribution of alpha-dystroglycan during embryonic nerve-muscle synaptogenesis. *J. Cell Biol.* **129**, 1093–1101 (1995).

22. Kim, N. *et al.* Lrp4 is a receptor for agrin and forms a complex with musk. *Cell* **135**, 334–342 (2008).

23. Apel, E. D., Glass, D. J., Moscoso, L. M., Yancopoulos, G. D. & Sanes, J. R. Rapsyn is required for MuSK signaling and recruits synaptic components to a MuSK-containing scaffold. *Neuron* **18**, 623–635 (1997).

24. Barik, A. *et al.* Lrp4 is critical for neuromuscular junction maintenance. *J. Neurosci.* **34**, 13892–13905 (2014).

25. Yumoto, N., Kim, N. & Burden, S. J. Lrp4 is a retrograde signal for presynaptic differentiation at neuromuscular synapses. *Nature* **489**, 438–442 (2012).

26. Fu, D. X. & Sine, S. M. Competitive antagonists bridge the alpha-gamma subunit interface of the acetylcholine receptor through quaternary ammonium-aromatic interactions. *J. Biol. Chem.* **269**, 26152–26157 (1994).

27. Tabuchi, K., Biederer, T., Butz, S. & Südhof, T. C. Cask participates in alternative tripartite complexes in which mint 1 competes for binding with caskin 1, a novel cask-binding protein. *J. Neurosci.* **22**, 4264–4273 (2002).

28. Südhof, T. C. Neuroligins and neurexins link synaptic function to cognitive disease. *Nature* **455**, 903–911 (2008).

29. Han, K. A. *et al.* Lar-rptps directly interact with neurexins to coordinate bidirectional assembly of molecular machineries. *J. Neurosci.* **40**, 8438–8462 (2020).

30. Tibbe, D., Pan, Y. E., Reißner, C., Harms, F. L. & Kreienkamp, H.-J. Functional analysis of CASK transcript variants expressed in human brain. *PLOS ONE* **16**, e0253223 (2021).

31. Hsueh, Y. P., Wang, T. F., Yang, F. C. & Sheng, M. Nuclear translocation and transcription regulation by the membrane-associated guanylate kinase CASK/LIN-2. *Nat. 2000 4046775* **404**, 298–302 (2000).

32. Huang, T.-N., Chang, H.-P. & Hsueh, Y.-P. CASK phosphorylation by PKA regulates the protein-protein interactions of CASK and expression of the NMDAR2b gene. *J. Neurochem.* **112**, 1562–1573 (2010).

33. Mukherjee, K. *et al.* CASK Functions as a Mg2+-Independent Neurexin Kinase. *Cell* **133**, 328–339 (2008).

Figures and legends

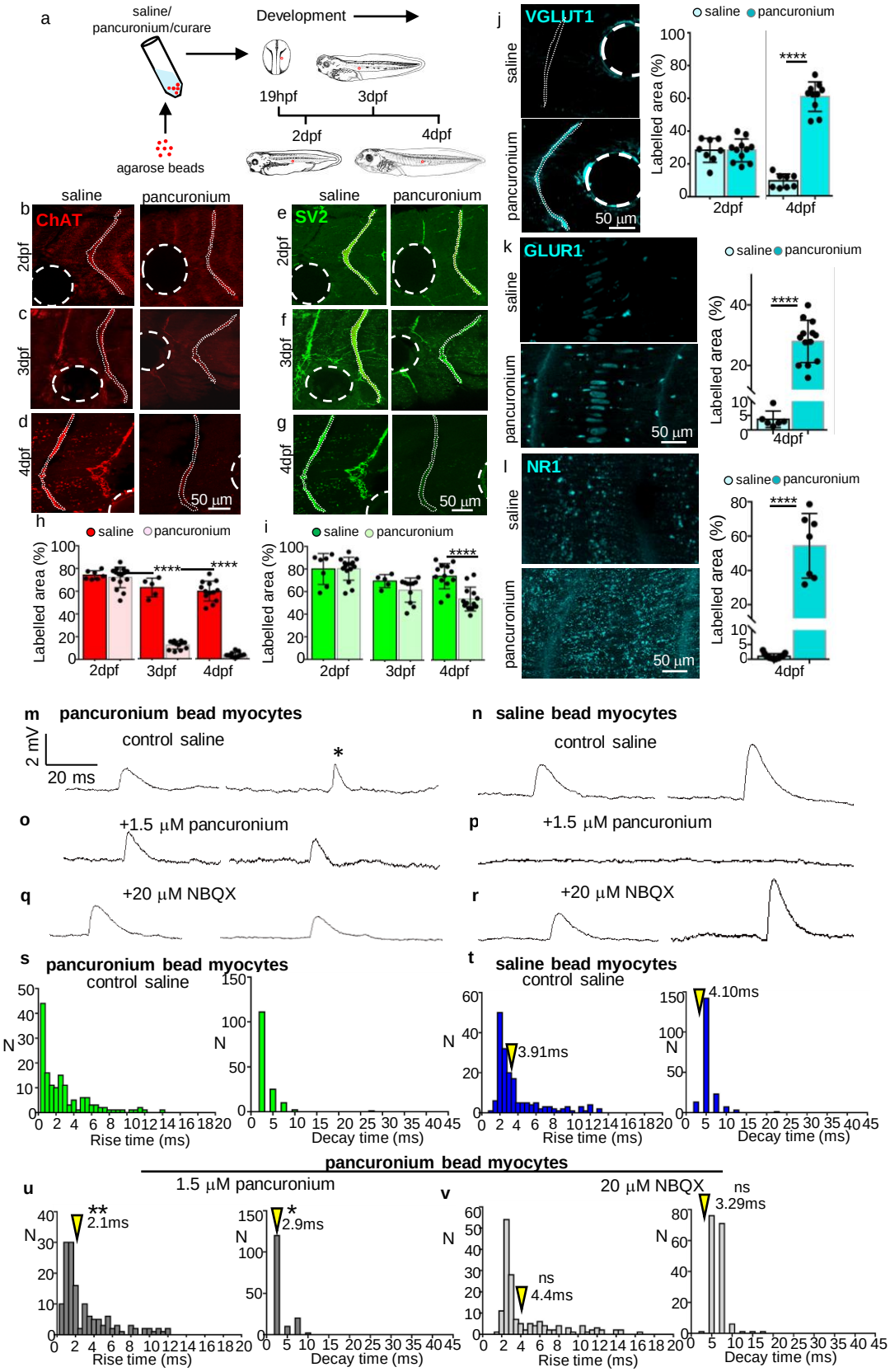

Fig 1. Local block of AChR in myocytes prior to NMJ formation reduces ChAT expression in innervating axons and induces a glutamatergic phenotype. (**a**) Schematic showing agarose beads loaded with saline (control), pancuronium or dTc implanted into the *Xenopus* mesoderm at 19hpf. Bead-implanted larvae were examined at 2dpf, 3dpf and 4dpf for ChAT and SV2 at 2dpf (**b, e**), 3dpf (**c, f**) and 4dpf (**d, g**). Area of expression is quantified for ChAT (**h**) and SV2 (**i**). Expression and quantification of VGLUT1 (**j**), GLUR1 (**k**) and NR1 (**l**) in myotome of control and pancuronium-loaded agarose bead-implanted larvae at 4dpf. White-dashed circles indicate positions of agarose beads. White-dotted lines outline myocommatal junctions analyzed for quantification of staining areas. ****p<0.0001, two-tailed t-test. **m)** Recordings from pancuronium-bead-implanted myocytes of 4dpf larvae reveal very fast-rise and very fast-decay mEPPs (asterisk) that are pancuronium-resistant (**o**) and NBQX-sensitive (**q**), as well as fast-rise and fast-decay mEPPs that are pancuronium-sensitive and NBQX-resistant. (**n**) Recordings from saline-bead-implanted myocytes reveal only pancuronium-sensitive fast-rise and fast decay mEPPs (**p, r**). Rise and decay time distributions for mEPPs in myocytes of pancuronium-bead implanted larvae (**s**) and saline-bead implanted larvae (**t**) in presence of saline. Rise and decay time distributions for mEPPs in myocytes of pancuronium-bead implanted larvae in presence of pancuronium (**u**) and NBQX (**v**). N, number of mEPPs. >155 mEPPs (≥3 tadpoles) for each group. Only mEPPs with decay times fit by single exponentials were included. Resting potentials were held near -60 mV. Arrowheads indicate mean values. Kolmogorov-Smirnov test compared rise time and decay time in (h) with respective rise and decay time in (i) and (j). *p<0.05, **p<0.01, ns not significant.

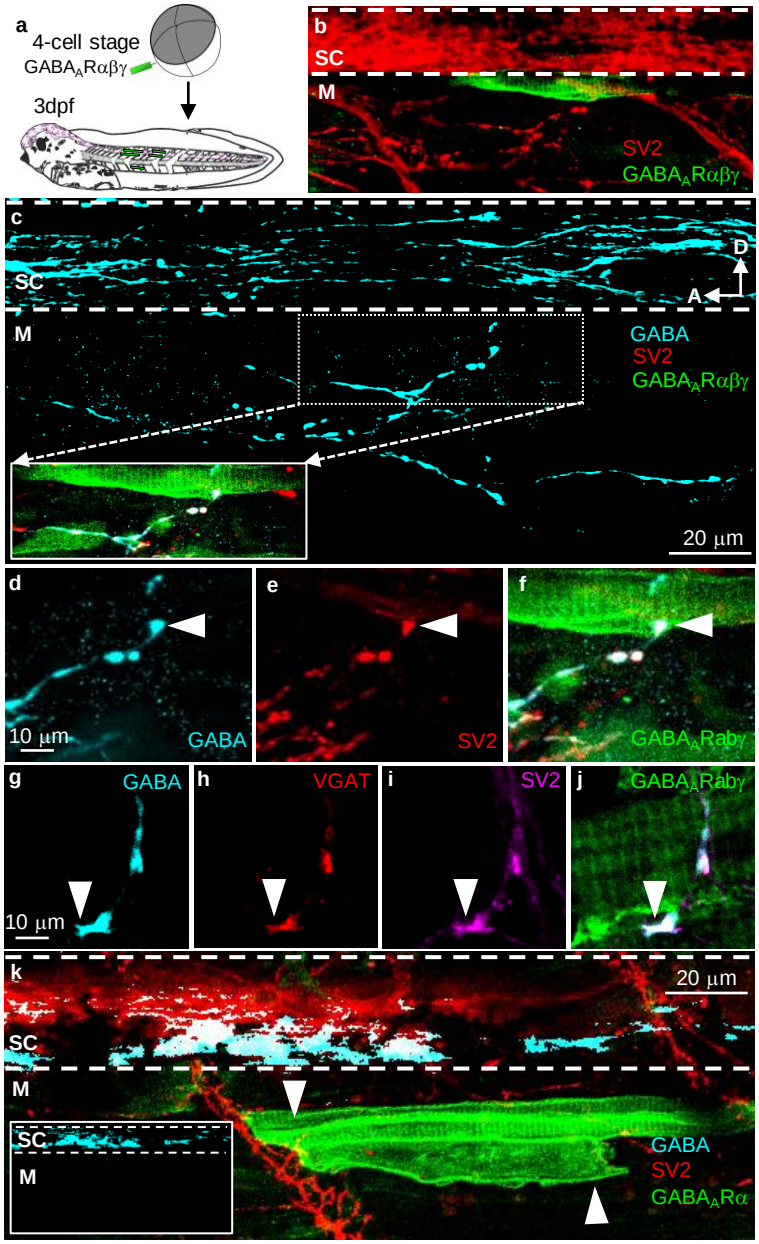

Fig 2. GABA$_A$Rαβγ expression in myocytes leads to GABA expression in axons that innervate them. (**a**) Injection of blastomere V2.1 with GABA$_A$Rαβγ mRNA results in myocyte-specific GABA$_A$R expression. (**b**) Sparse expression of GABA$_A$Rαβγ in the trunk myotome (M). SV2 labels neuronal axons in the spinal cord (SC) and in the trunk myotome (M). (**c**) In the same field of view, staining for GABA reveals GABA+ axons in the spinal cord (SC) and coursing ventrally and posteriorly over the trunk myotome (M). D- dorsal, A- anterior. *Inset:* A GABA+SV2+ axon contacts a GABA$_A$Rαβγ-expressing GFP+ myocyte (white box). 3dpf. (**d-f**) Higher magnification of contact in (**c**) (white arrowheads). (**g-j**) A GABA+VGAT+SV2+ axon contacts a different GABA$_A$Rαβγ myocyte. 3dpf. (**k**) Injection of blastomere V2.1 with GABA$_A$Rα mRNA results in sparse expression of GABA$_A$Rα in the trunk myotome (M). SV2+ axons contact a GABA$_A$Rα-expressing GFP+ myocyte (white arrowheads). *Inset,* GABA+ axons are restricted to the spinal cord (SC).

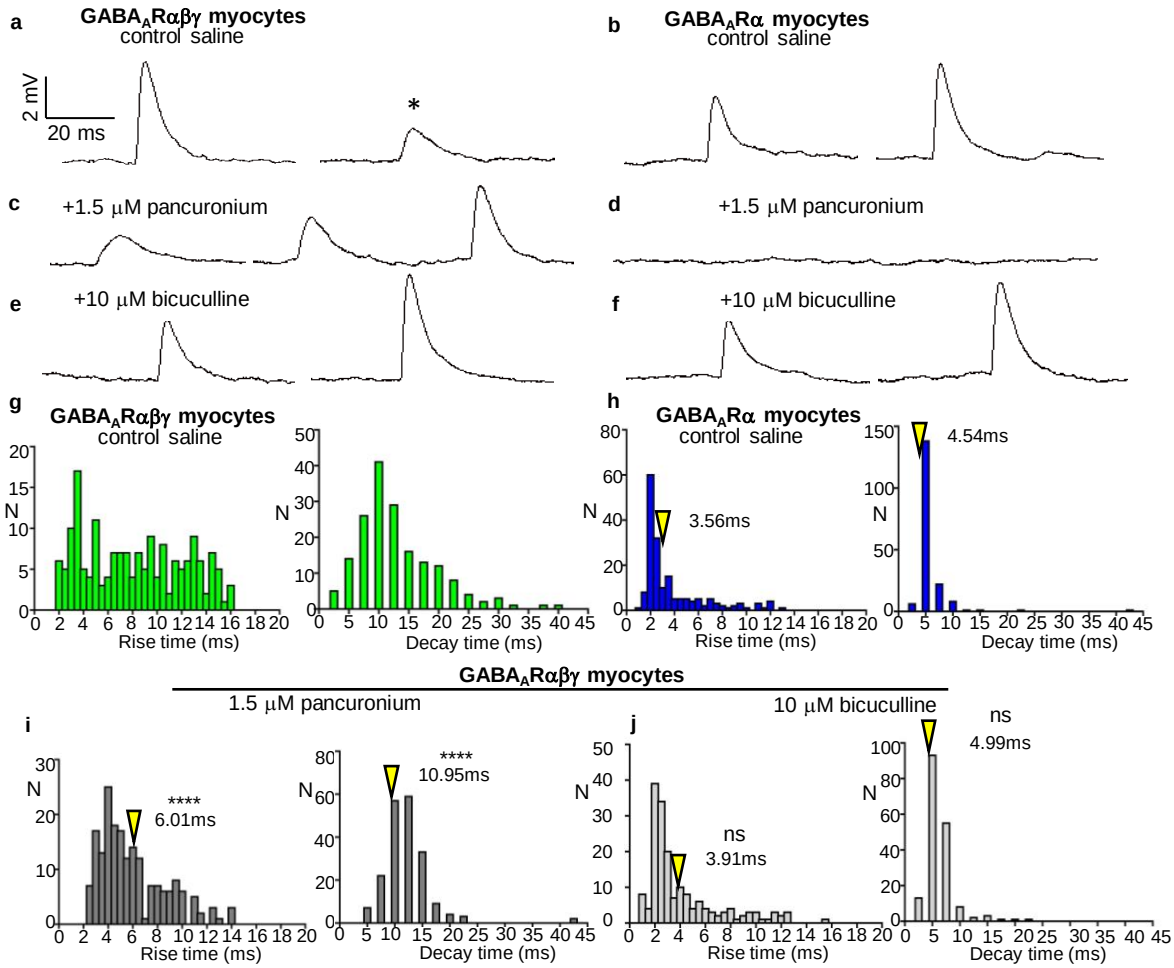

Fig 3. Neuromuscular junctions expressing GABA$_A$Rαβγ generate GABAergic and cholinergic mEPPs. a) Recordings from GABA$_A$Rαβγ myocytes of 4dpf larvae reveal slow-rise and slow-decay mEPPs (asterisk) that are pancuronium-resistant (**c**) and bicuculline-sensitive (**e**), as well as fast-rise and fast-decay mEPPs that are pancuronium-sensitive and bicuculline-resistant. (**b**) Recordings from GABA$_A$Rα myocytes reveal only pancuronium-sensitive fast-rise and fast decay mEPPs (**d, f**). Rise and decay time distributions for mEPPs in GFP+ myocytes of GABA$_A$Rαβγ larvae (**g**) and GABA$_A$Rα larvae (**h**) in presence of saline. Rise and decay time distributions for mEPPs in GFP+ myocytes of GABA$_A$Rαβγ larvae in presence of pancuronium (**i**) and bicuculline (**j**). N, number of mEPPs. >178 mEPPs (≥5 tadpoles) for each group. Only mEPPs with decay times fit by single exponentials were included. Resting potentials were held near -60 mV. Arrowheads indicate mean values. Kolmogorov-Smirnov test comparing rise time and decay time in (h) with respective rise and decay time in (i) and (j). ****$p<0.0001$, ns not significant.

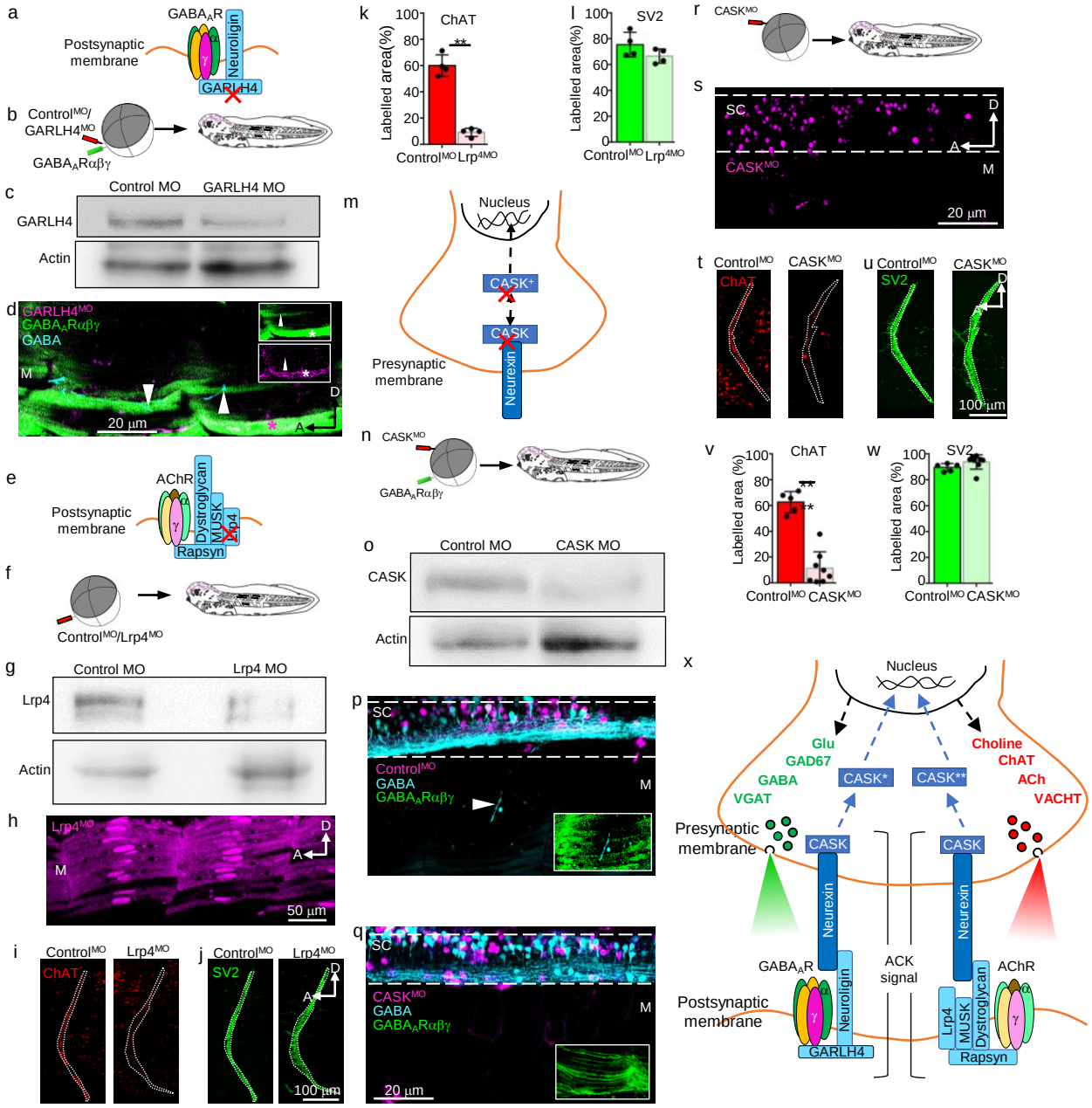

Fig 4. Receptor-driven neurotransmitter stabilization is mediated by transsynaptic bridges. (**a**) GARLH4 links GABA$_A$Rαβγ to neuroligin in the postsynaptic membrane. (**b**) Staggered injection of ventral blastomere 2.1 with GABA$_A$Rαβγ mRNA followed by low dose of control^{MO} or GARLH4^{MO}. (**c**) Presence of GARLH4 and morpholino knockdown validation by western blot. (**d**) Axons contacting GABARαβγ myocytes express GABA (arrowheads; 5/5). Axons contacting a GARLH4^{MO} GABA$_A$Rαβγ myocyte do not express GABA (asterisk, 0/12). *Insets,* individual channels for GFP (GABARαβγ) and GARLH4^{MO}. (**e**) Lrp4 links to AChR through rapsyn and to MUSK and dystroglycan in the postsynaptic membrane. (**f**) Injection of ventral blastomere 2.1 with a high dose of Lrp4^{MO} or control^{MO}. (**g**) Morpholino knockdown validation by western blot. (**h**) Lrp4^{MO} expression in the myotome of a 3dpf larva. (**i, j**) Myocommatal junctions of larvae with control or Lrp4^{MO} stained for ChAT and SV2 at 3dpf. (**k, l**) Intensity of expression quantified for ChAT and SV2. n=4, **p=0.0092, two-tailed *t-test*. (**m**) CASK links to neurexin. (**n**) Injection of GABARαβγ RNA in ventral blastomere 2.1 and a high dose of CASK^{MO} in dorsal blastomere 1.2. (**o**) Presence of CASK and morpholino knockdown validation by western blot. (**p**) GABA axon in myotome of 3dpf control^{MO} GABARαβγ larva (arrowhead, 6/6). (**q**) 3dpf CASK^{MO} GABARαβγ larvae do not show GABA expression in the myotome (0/12). (**r**) Injection of CASK^{MO} in dorsal blastomere 1.2. (**s**) 3dpf larva expressing CASK^{MO} in SC. (**t, u**) Myocommatal junctions of larvae with control^{MO} or CASK^{MO} examined for ChAT and SV2. (**v, w**) Intensity of expression quantified for ChAT and SV2. n≥5, ****p<0.0001, two-tailed *t-test*. (**x**) Summary of interactions between neurotransmitter receptors and transsynaptic bridge proteins that convey retrograde ACK signals to achieve presynaptic transmitter stabilization. n/N, larvae with GABA+ axon/total larvae observed. Red X in a,e and m, protein knocked-down. M, myotome; SC, spinal cord; NT- neurotransmitter. D, dorsal; A, anterior.

Methods

Animals

Frogs were purchased from Nasco and Xenopus 1 and maintained on the daily light-dark cycle. Adult female frogs were primed with 10 IU human chorionic gonadotropin (HCG; Millipore Sigma) 1 week prior to collection of eggs. Testes were harvested and stored in 20% fetal bovine serum or were cryopreserved till fertilization[1]. Ovulation was induced by injection of 500 IU HCG 12 hr prior to egg collection and fertilization. Eggs were fertilized *in vitro* and embryos were grown in 0.1X Marc's modified Ringer's solution (MMR: 100 mM NaCl, 2 mM KCl, 1 mM $MgSO_4$, 5 mM HEPES, 0.1 mM EDTA, 2 mM $CaCl_2$, pH 7.8). Developmental stages were determined from developmental tables[2,3]. All animal procedures were performed in accordance with institutional guidelines and approved by the UCSD Institutional Animal Care and Use Committee.

Local drug delivery

Spatial and temporal control of delivery of pharmacological agents was achieved using agarose beads (100-200 mesh, Bio-Rad)[4,5]. Beads were washed in 2 mM Ca^{2+} medium for 3 h at 22°C, replacing washing solution every 20 min, and loaded for 2 h at 4°C on a bi-directional rotator with 2 mM Ca^{2+} medium containing drugs (30 μM pancuronium (Fisher Scientific), or 38.9 μM curare (Sigma-Aldrich), or saline (0.9% sodium chloride; stock solutions of drugs were diluted in saline). Drug concentrations were 10X the concentration tested in myocyte cultures[4,5], to compensate for dilution during diffusion. Beads of 120 μm diameter were selected and implanted into the mesoderm (120 μm from the neural tube) ~400 μm behind the eye primordium at 20 hpf (stage 18), allowed to develop in 0.1X MMR to 2 dpf (Stage 35), 3 dpf (St 41) or 4 dpf (St 43), and processed for immunohistochemistry. Each experimental group contained 4-8 bead- implanted embryos. Only myocommatal junctions within ~100 μm of a bead were considered for analysis.

Whole mount immunohistochemistry

Whole *Xenopus* larvae were fixed at the indicated stages of development in 4% PFA and 0.1% glutaraldehyde for 1 h. After 3 washes in 1X PBS, the epidermis and head of fixed larvae were removed in 1X PBS and the larvae were transferred into a 12-well plate containing blocking solution (5% normal donkey serum, 1% fish gelatin, 0.5% Triton-100 in 1X PBS) for 1 h. Larvae

were then transferred to fresh wells containing primary antibodies diluted in 50% blocking solution in 1X PBS and incubated at 4°C for 3 d. Antibodies used were ChAT (1:500, Millipore, AB144P), SV2 (1:500, Developmental Studies Hybridoma Bank, AB2315387), VGLUT1 (1:200, Millipore, AB5905), GLUR1 (1:200, MilliporeSigma, MAB2263), NR1 (1:200, MilliporeSigma, MAB363), GABA (1:200, Millipore, ABN131), VGAT (1:300, cytoplasmic domain, Synaptic Systems, 131013), GFP (1:500, Synaptic Systems, 132005), Hb9 (1:10, Developmental Studies Hybridoma Bank, 81.5C10), GAD67 (1:250, Millipore, MAB5406), Glycine (1:200, Millipore, AB139), Lim3 (1:200, Millipore, AB3202), rAldh1a2 (1:8000, ZMBBI Columbia, CU1022), pan-Neurexin (1:200, kind gift from Peter Scheiffele), pan-Neuroligin (1:200, Invitrogen, PA5-77523). After 3 washes in 1X PBS, larvae were incubated in the dark at 4°C for 24 h with secondary antibodies (1:500, Alexa Fluors 488, 555, 594 and 647, Jackson Immunoresearch). Following 3 washes with 1X PBS, larvae were serially dehydrated in 50% methanol and 100% methanol for clearing with BABB (Benzyl alcohol:benzyl benzoate 1:2, Sigma-Aldrich) for 24 h at 4°C. After 24 h the larvae were transferred to wells containing fresh BABB and reincubated for 24 h. Larvae were mounted onto slides with the side exhibiting maximum expression facing up. Confocal images of whole larvae were acquired on a Leica Stellaris 8 confocal microscope with 25x/0.95 water immersion objective, at a z-resolution of 0.5 μm and analyzed with FIJI. Imaging parameters were kept constant within each experiment.

Image analysis

Analysis of myocommatal junctions: For each larva the first optical slice exhibiting SV2 expression at the myocommatal junction was determined and optical slices were stacked from that slice onwards to obtain 25 μm thick maximum intensity projections. These projections enabled examination without contamination of the signal by SV2 processes in the spinal cord. The ROIs for the myocommatal junctions were outlined with the FIJI freehand selection tool using the SV2 signal as reference. The SV2 and ChAT or VGLUT1 images were converted into 8-bit format and then into binary images. The percentage area in the ROI labelled with the signal was measured for SV2 and ChAT or VGLUT1. Data analysis parameters were kept constant within each experiment, allowing aggregation of data from independent batches of larvae. For bead-

implantation experiments, myocommatal junctions immediately anterior or posterior to the bead were analysed.

Analysis of myocytes between two myocommatal junctions, spanning one chevron: For each larva the first optical slice exhibiting GLUR1 or NR1 staining was determined, and optical slices were stacked from that slice onwards to generate 25 μm thick maximum intensity projections; these enabled examination of the myocytes in a chevron before the appearance of spinal cord that could otherwise obscure visibility of the axons of motor neurons. The percentage labelled area analysis of whole mount immunostained preparations included myocytes spanning one chevron immediately caudal to the bead, but excluded tissue edges, damaged cells, residual skin and pigment cells. Data were analyzed as described above.

Analysis of axons expressing GABA along the A-P axis: 20 3dpf GABARαβγ-expressing larvae were examined along the entire length of their anterior-posterior axis. When a terminal axon expressing GABA was detected in the myotome of a larva, its chevron position was determined, and the position of the axon was marked on a schematic of a 3dpf larva using the ImageJ multipoint tool. These points were saved as a region of interest (ROI). All the ROIs were overlaid together on the 3dpf schematic to determine if there was an A-P distribution preference for these axons in the myotome. Chevrons along the schematic were broadly divided into three groups for the purpose of analysis- anterior (light blue): chevrons 1 to 7, middle (blue): chevrons 8 to 16, and posterior (dark blue): chevrons 17 to 21.

Cell counting

FIJI software was used for fluorescent cell counting and all slices within the confocal stack were examined without maximal projection. Immunoreactive cells were counted from at least 3 different larva per treatment ($GABA_AR\alpha$ or $GABA_AR\alpha\beta\gamma$). Representative images are maximum intensity projections of 5 consecutive slices.

Plasmids and morpholinos

$GABA_AR$ subunits α1-EGFP, β2 and γ2 were generated in the Czajkowski lab[6]. The $GABA_AR$ subunits were subcloned into pCS2 by VectorBuilder (Santa Clara, CA)- pCS2-GABAr alpha-GFP

VB180118-1043eef, pCS2 GABAr beta VB180303-1004bat, pCS2 GABAr gamma VB180303-1005aab. The lissamine-tagged GARLH4, Lrp4 and CASK morpholinos were supplied by GeneTools (Philomath, OR) (GARLH4 MO1 5'-TTCTTGTGAAGTCAACATCTTGG-3', GARLH4 MO2 5'-GAGTCCTCACTCAGTATCC-3', GARLH4 negative control MO 5'- GGTTCTACAACTGAAGTGTTCTT-3', Lrp4 MO 5'- CCCATAATGCCACTTCTCC-3', Lrp4 negative control MO 5'- CCTCTTCACCGTAATACCC-3', CASK MO 5'-GGGTTTAACACCACCACAAAGGA-3', standard control oligo 5'-CCTCTTACCTCAGTTACAATTTATA-3').

Microinjections

Plasmids were amplified with the Qiagen miniprep kit and linearized with Not1-HF (New England Biolabs). α1-EGFP, β2 and γ2 capped mRNA were transcribed using the mMessage mMachine SP6 kit (Invitrogen). The integrity of the mRNA was assessed using both Nanodrop and agarose gel electrophoresis. On the day of microinjections, oocytes were fertilized in 0.1X MMR and 20 min later treated in 2% cysteine (Sigma-Aldrich) to remove the jelly coat. They were rinsed 10 times in 0.1X MMR and allowed to develop to the 4-cell stage in 0.1X MMR at 25°C. Embryos were transferred to 6% Ficoll (Sigma-Aldrich) for injections. Using Picospritzer III, α1, β2 and γ2 mRNA were co-injected in 1:1:1 ratio along with phenol red (to visualize the solution) into the ventral blastomere 2.1 (V2.1) to a total volume of 3 nl to target expression to myocytes[7]. 6 nl of 1 mM Lrp4 MO and 1 nl or 3 nl of 1mM GARLH4 MO or their respective control morpholinos were injected into the ventral blastomere to knockdown the respective mRNAs. 6 nl of 1mM CASK MO or its control morpholino were injected into the dorsal blastomere 1.2 (D1.2) at the 16 cell stage to target expression in the spinal cord[8]. Higher doses of Lrp4 MO and CASK MO were delivered to achieve widespread knock-down of the Lrp4 and CASK, as strong changes in phenotype were not observed at 3nl dose. 3 nl of 1mM GARLH4 labelled almost all myocytes. This dose along with GABAR$\alpha\beta\gamma$ mRNA injection was used to test the necessity of GARLH4, while the low dose of GARLH4 MO followed by GABAR$\alpha\beta\gamma$ mRNA injection was used to achieve sparse labelling of myocytes with the morpholino. Injected embryos were transferred to 0.1X MMR and developed at 25°C. Lissamine was detected immediately post-injection, while GFP fluorescence was detected 17hpf (St 15) as previously reported[9], and persisted up to 7 dpf (St 48).

Protein extraction and elisa

Larvae were anaesthetised in tricaine methanesulphonate (diluted 1:2 in water) for 1 min, skinned and gut removed using jewellers' forceps. Larvae were secured to Sylgard in a 60 mm plastic Petri dish with a minutien pin (dorsal side up). The melanocyte layer covering the dorsal side (spinal cord) was gently removed. 0.05% collagenase was added to the dorsal side of the larva using a glass capillary, for 5 min. The collagenase was then removed and replaced with 1XPBS. The brain and spinal cord were lifted out, collected into a 2 ml Eppendorf and frozen immediately in liquid nitrogen. The trunk myotome was collected in another Eppendorf and frozen the same way. Thirty brains and spinal cords were pooled for a single experiment to yield sufficient protein. Samples were sonicated in RIPA lysis buffer (150 mM NaCl, 50 mM Tris (pH 7.4), 2 mM EDTA, 1% NP-40, 0.1% SDS, 0.1 % (v/v) Protease Inhibitor) and cell debris was pelleted by centrifugation at 5000xg for 10 min. Protein concentration of the supernantant was estimated using the BCA method (ThermoFisher). ELISA assays were performed per the manufacturer's instructions (GFP ELISA Kit, Cell Biolabs).

Mesoderm grafting

To obtain myocyte-specific $GABA_AR\alpha\beta\gamma$ or $GABA_AR\alpha$ expression, presomite mesoderm of wild-type embryos 15 hpf (St 13-14) was replaced with presomite mesoderm explant dissected from sibling embryos expressing either $GABA_AR\alpha\beta\gamma$ or $GABA_AR\alpha$ transcripts. The grafting technique was similar to that previously described[10]. Briefly, embryos were manually demembranated with jeweller's forceps, then incised using a tungsten needle in the posterior region next to the blastopore, at the level of the presumptive tail-forming region. The neural plate was cut laterally, left attached at the midline and lifted using a hair loop to free access to the underlying presomitic mesoderm. To immobilise the graft and promote healing, the operated region was covered by a small glass coverslip bridge. The grafted embryos were allowed to heal under these bridges and then moved to 0.1X MMR for further development.

Electrophysiology

Sample Preparation: 4 dpf (St 43) larvae were anaesthetized in ice cold 10% MMR. After ensuring non-responsiveness to touch, a larva was transferred into a 60 mm Petri dish with ice cold external solution and the epidermis peeled back using sharp forceps to expose the trunk myotome. The larva was moved to a Sylgard platform (~1 mm thick) in the same Petri dish and glued laterally in place with Vetbond tissue adhesive (3M). A glass capillary and mouth pipette were used to apply a drop of Vetbond glue to Sylgard. The Sylgard platform with the larva was transferred into a recording chamber containing external solution (NaCl 115 mM, KCl 4 mM, $CaCl_2$ 3 mM, $MgCl_2$ 1 mM, HEPES 5 mM, D-Glucose 10 mM; pH 7.2, Osm 250-255).

Sharp electrode recording: G150F-3 (borosilicate: standard wall with filament) capillaries were loaded with internal solution (3 M KCl) through microfil/microloader tips. The filled-capillaries were placed upside-down (sharp side down) on plasticine stuck to the edge of a shelf for gravity-assisted removal of air bubbles. Glass pipettes with resistance of 54-75 MΩ were used for recordings. Myocytes, identified by the presence of sarcomeres visualized with an upright Zeiss microscope and a water immersion 40Xx/0.8 objective, were impaled within 40 μm of the myocommatal junction for recordings. Multiclamp 7008, Clampex 10.7 software and Clampfit 10.7 data interfaces were used for acquisition and analysis of miniature postsynaptic end-plate potentials (mEPPs). The membrane potential was held at -60 mV with bridge balance for the duration of recordings. mEPPs were recorded for a duration of 5 min, after which blockers (pancuronium 1.5 μM, bicuculline 10 μM, NBQX 20 μM, AP5 40 μM) were perfused into the recording chamber (2 ml/min). Following 10 min of perfusion mEPPs were recorded in the presence of the blockers to determine receptor dependence. Blockers were judged effective when they reversibly reduced the frequency and amplitude of mEPPs. The drugs were washed out for 20 min and recovery mEPPs recorded to ensure the sample preparation was healthy throughout the recording. The recordings from bead-implanted larvae and morpholino-injected larvae were performed in the presence of 1 μM tetrodotoxin to prevent contribution of off-target effects of pancuronium or NBQX. Rise times were scored from 10% to 90% of peak and decay times were determined by fitting exponentials with the MiniAnalysis program (Synaptosoft Inc, Decatur, GA). The rise and decay time distributions in different conditions were compared using

Kolmogorov-Smirnov test and considered significantly different when $P < 0.05$. Frequencies were scored as mEPPs min^{-1} and considered significantly different when $P < 0.05$.

Western blotting

Protein for western blotting was extracted as described above except that the larvae were anaesthetized on ice and RIPA lysis buffer was supplemented with phosphatase inhibitors (PhosSTOP, Roche). 30 μg of total protein were used and Ponceau S staining was used to check total protein levels on the membrane. Protein detection by western blotting was performed for Lrp4 (1:8000, extracellular domain, generous gift from Stephan Kröger), GARLH4 (1:500, LifeSpan Biosciences, LS-C170010), CASK (1:500, Santa Cruz Biotechnology, SC-13158). The same blots were re-probed for the loading control actin (1:1000, Sigma-Aldrich, A2066-100UL). Signal was detected using Clarity ECL western substrate (BioRad) and imaged on a BioRad Chemidoc Touch Imaging System.

Statistics

Values were expressed as mean ± SD. Statistical differences were analysed using the unpaired, two-tailed Student's *t-test*. The statistical test used and the P values for each measurement are provided in the figures or figure legends. $P<0.05$ was considered statistically significant. All statistical analysis was performed in GraphPad Prism.

Methods references

1. Noble, A., Abu-Daya, A. & Guille, M. Cryopreservation of *Xenopus* sperm and in vitro fertilization using frozen sperm samples. *Cold Spring Harb. Protoc.* **2022**, pdb.prot107029 (2022).
2. *Normal table of Xenopus laevis (daudin): a systematical and chronological survey of the development from the fertilized egg till the end of metamorphosis*. (Garland Pub, 1994).

3. Segerdell, E. *et al.* Enhanced XAO: the ontology of *Xenopus* anatomy and development underpins more accurate annotation of gene expression and queries on Xenbase. *J. Biomed. Semant.* **4**, 31 (2013).
4. Hammond-Weinberger, D. R., Wang, Y., Glavis-Bloom, A. & Spitzer, N. C. Mechanism for neurotransmitter-receptor matching. *Proc. Natl. Acad. Sci.* **117**, 4368–4374 (2020).
5. Root, C. M., Velázquez-Ulloa, N. A., Monsalve, G. C., Minakova, E. & Spitzer, N. C. Embryonically expressed gaba and glutamate drive electrical activity regulating neurotransmitter specification. *J. Neurosci.* **28**, 4777–4784 (2008).
6. Connor, J. X., Boileau, A. J. & Czajkowski, C. A GABAA receptor alpha1 subunit tagged with green fluorescent protein requires a beta subunit for functional surface expression. *J. Biol. Chem.* **273**, 28906–11 (1998).
7. Moody, S. A. & Kline, M. J. Segregation of fate during cleavage of frog (*Xenopus laevis*) blastomeres. *Anat. Embryol. (Berl.)* **182**, 347–362 (1990).
8. Moody, S. A. Fates of the blastomeres of the 16-cell stage *Xenopus* embryo. *Dev. Biol.* **119**, 560–578 (1987).
9. Guemez-Gamboa, A., Xu, L., Meng, D. & Spitzer, N. C. Non-cell-autonomous mechanism of activity-dependent neurotransmitter switching. *Neuron* **82**, 1004–1016 (2014).
10. Gargioli, C. & Slack, J. M. W. Cell lineage tracing during *Xenopus* tail regeneration. *Development* **131**, 2669–2679 (2004).

Acknowledgements
We thank all members of the Spitzer laboratory for discussions and critical feedback; K. Marek for discussions of acknowledgement signals; I. Gregor and R. Aricescu for discussions of receptor pharmacology and transsynaptic bridges; C. Kintner for advice on *Xenopus* blastomere lineage; A. Ray and E. Park for guidance on miniature analysis; A. Glavis-Bloom, S.U. Choi and S. Malladi for technical assistance; D.K. Berg and L.R. Squire for comments on the manuscript. This work was supported by NSF 2051555 and the Overland Foundation.

Author information
Author contributions
S.K.G and N.C.S conceived the study and designed the experiments with input from H.L. and M.P. S.K.G. performed all the experiments. M.H. and H.T.C. performed electrophysiology experiments with S.K.G. Y.I. and L.S. contributed to the identification of motor neuron identity. J.B. and C.C. contributed $GABA_A$ receptor clones and advice regarding expression. J.B.L and L.N.B provided instruction in embryonic tissue transplantation. S.K.G. and N.C.S wrote the manuscript with contributions from all authors.

Corresponding authors
Correspondence to Swetha K. Godavarthi- skgodavarthi@ucsd.edu or Nicholas C. Spitzer- nspitzer@ucsd.edu

Ethics declaration
Competing interests
The authors declare no competing interests.

Additional Information
Supplementary information- Suppl Fig 1 to Suppl Fig 20